Journal of Sound and Vibration (2002) **251**(1), 59–78
doi:10.1006/jsvi.2001.3984, available online at http://www.idealibrary.com on IDEAL®

FREE VIBRATION ANALYSIS OF A SPINNING FLEXIBLE DISK–SPINDLE SYSTEM SUPPORTED BY BALL BEARING AND FLEXIBLE SHAFT USING THE FINITE ELEMENT METHOD AND SUBSTRUCTURE SYNTHESIS

G. H. JANG AND S. H. LEE

PREM, Department of Mechanical Engineering, Hanyang University, Haengdang-Dong, Sungdong-Gu, Seoul, 133-791, *Korea. E-mail:ghjang@hanyang.ac.kr*

AND

M. S. JUNG

Digital Audio/video Division, LG Electronics Inc. 19-1, *Cheongho-Ri, Jinwi-Myeon, Pyungtaik-City, Kyunggi-Do*, 451-713, *Korea*

(*Received* 4 *May* 2001, *and in final form* 26 *July* 2001)

Free vibration of a spinning flexible disk–spindle system supported by ball bearing and flexible shaft is analyzed by using Hamilton's principle, FEM and substructure synthesis. The spinning disk is described by using the Kirchhoff plate theory and von Karman non-linear strain. The rotating spindle and stationary shaft are modelled by Rayleigh beam and Euler beam respectively. Using Hamilton's principle and including the rigid body translation and tilting motion, partial differential equations of motion of the spinning flexible disk and spindle are derived consistently to satisfy the geometric compatibility in the internal boundary between substructures. FEM is used to discretize the derived governing equations, and substructure synthesis is introduced to assemble each component of the disk–spindle–bearing–shaft system. The developed method is applied to the spindle system of a computer hard disk drive with three disks, and modal testing is performed to verify the simulation results. The simulation result agrees very well with the experimental one. This research investigates critical design parameters in an HDD spindle system, i.e., the non-linearity of a spinning disk and the flexibility and boundary condition of a stationary shaft, to predict the free vibration characteristics accurately. The proposed method may be effectively applied to predict the vibration characteristics of a spinning flexible disk–spindle system supported by ball bearing and flexible shaft in the various forms of computer storage device, i.e., FDD, CD, HDD and DVD.

1. INTRODUCTION

The spinning disk–spindle system supported by bearing and flexible shaft has been widely used in various forms of computer storage devices, i.e., FDD, CD, HDD and DVD. Figure 1 shows the HDD spindle system. Vibration of the spinning disk–spindle system determines the performance of these devices. Particularly, vibration of the disk–spindle system in HDD plays the major role in the determination of the disk memory capacity because the servo system cannot position the recording head back to the data track if the in-plane vibration exceeds the allowable track misregistration, approximately 5% of data track pitch. At the end of 2000, magnetic track density is around 40 000 TPI (track/in) – that

0022-460X/02/110059 + 20 $35.00/0

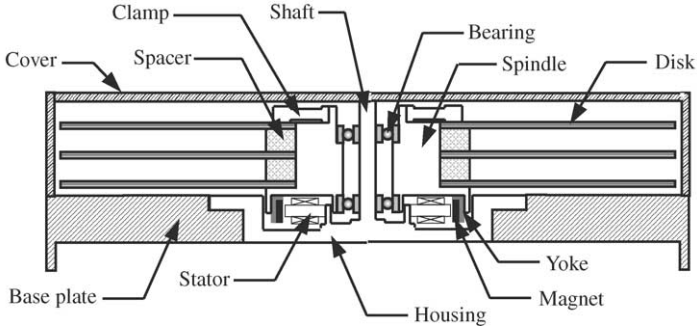

Figure 1. Disk–spindle–bearing–shaft sytem in an HDD.

requires a non-repeatable vibration smaller than 0·03 μm. As computer storage devices are getting smaller, thinner and faster, it is becoming important to predict the vibration characteristics of the disk–spindle system accurately.

Many papers have been presented on the free vibration analysis of the spinning flexible disk–spindle system since Dopkin and Shoup [1] showed that disk flexibility decreases the first natural frequency of the rotating shaft significantly. Recently, many researchers have investigated the dynamics of the spinning flexible disk–spindle system in computer storage devices considering the modal interaction between a flexible spinning disk and spindle. Shen and Ku [2] analyzed the free vibrations of a spinning elastic disk and rigid spindle system by the assumed mode method, and they investigated the modal coupling of hard disk drives. They did not include the flexibility of the stationary shaft so that they did not fully explain the discrepancy of the rocking mode frequency between the theoretical prediction and modal testing. Lee and Chun [3, 4] also analyzed the natural frequencies of the coupled flexible spinning disk–spindle system by using the assumed mode method and substructure synthesis. Their analyses also did not include the flexibility of the stationary shaft. The previous works [2–4] described the disk motion as the generalized co-ordinates using Lagrange's method, that is, the governing equations of a spinning disk are expressed as the discretized form using generalized co-ordinates. Assumed mode method has the advantage of having small number of degrees of freedom, but it cannot be appropriately applied to the problem including a complex geometry or boundary in which admissible functions cannot be obtained.

On the other hand, Lim [5] has investigated the dynamics of the spinning flexible disk–spindle system by using the finite element method and substructure synthesis. He described the disk with a linear model and he did not include the flexibility of the stationary shaft. He also used the Lagrange's method to derive the finite element equations. In the finite element method, the vibration mode does not have to be assumed, but it has more degrees of freedom than the assumed mode method. Equations of motion of each component also have to be consistently derived to satisfy the geometric compatibility in the internal boundary between substructures when the problem involves several components. However, the finite element method with substructure synthesis may be one of the powerful methods to analyze the vibration characteristics of the spinning flexible disk–spindle–bearing–shaft system once the equations of motion of each substructure are derived consistently.

In this paper, partial differential equations of motion of the spinning flexible disk including the rigid body motion are derived consistently to satisfy the geometric compatibility in the internal boundary between substructures by using Hamilton's

principle. FEM is used to discretize the derived governing equations, and substructure synthesis is introduced to assemble each component of the disk–spindle–bearing–shaft system. The developed method is applied to analyze the vibration characteristics of the spindle system of an HDD including every component of disk–spindle–bearing–shaft, and modal testing is performed to verify the accuracy and effectiveness of the proposed approach. It also investigates the natural frequencies of the disk–spindle–bearing–shaft system due to the effect of the spindle and shaft flexibility.

2. EQUATIONS OF MOTION

Governing equations of each substructure in the disk–spindle–bearing–shaft system have to be derived with the introduction of consistent variables to satisfy the geometric compatibility at the internal boundaries. Ball bearing restrains the spinning motion of the disk–spindle system in five degrees of freedom, i.e., displacement in x, y and z directions and the rotation in x and y directions. Motion of the rotating spindle and shaft can be described by Rayleigh and Euler beam including the axial rigid motion to satisfy the geometric compatibility in the spindle–bearing interface and the bearing–shaft interface respectively. Motion of the spinning disk can be superposed by its rigid body motion measured from the fixed co-ordinate and its elastic deformation, i.e., in-plane and transverse elastic displacement, measured from the rotating co-ordinate system. Introducing the rigid body motion of the spinning disk can satisfy the geometric compatibility between the disk and spindle interface. Table 1 shows the variables introduced in the disk–spindle–bearing–shaft system in order to analyze the free vibration of the disk–spindle–bearing–shaft system by using the finite element method and substructure synthesis.

2.1. EQUATIONS OF MOTION OF A SPINNING DISK WITH THE INFINITESIMAL RIGID BODY MOTION AND ELASTIC DEFORMATION

Figure 2 shows the spinning flexible disk with a constant angular speed Ω, and it undergoes the infinitesimal rigid body motion as well as the elastic deformation. The local reference frame, $x_2y_2z_2$ is located at the center of the disk after it has the infinitesimal rigid body translation and tilting motion with respect to the inertial reference frame, $x_1y_1z_1$, and the elastic deformation of the disk is observed with respect to this local reference frame.

TABLE 1

Variables in a disk–spindle–bearing–shaft system to satisfy the geometric compatibility

Co-ordinate	Motion	Disk	Spindle	Shaft
Fixed co-ordinate	x-displacement	X	u	u
	y-displacement	Y	v	v
	z-displacement	Z	Z	Z
	x-rotation	θ_x	$-\partial v/\partial x$	$-\partial v/\partial x$
	y-rotation	θ_y	$\partial u/\partial y$	$\partial u/\partial y$
Rotating co-ordinate	x-displacement	u		
	z-displacement	w		

Note: X, Y, Z, θ_x, θ_y: variables corresponding to the rigid body motion. u, v, w: variables corresponding to the elastic deformation.

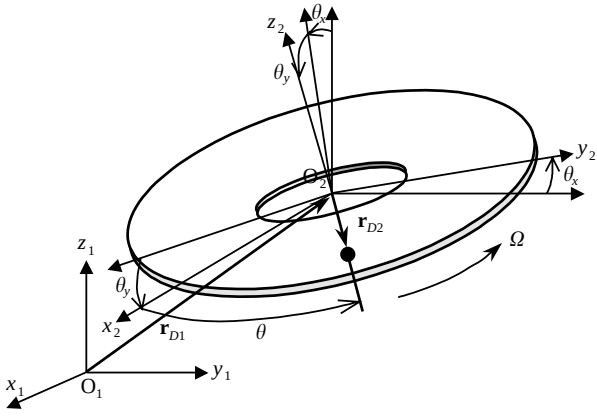

Figure 2. Spinning elastic disk with rigid body motions.

If the rotational speed of a disk is constant, it can be reasonably assumed that the radial displacement of a disk is axisymmetric and the circumferential displacement is negligible. With this assumption, the displacements of a disk are expressed by the Kirchhoff plate theory as follows:

$$u_r(r, \theta, z, t) = u_D(r) - z\frac{\partial w_D(r, \theta, t)}{\partial r},$$
$$u_\theta(r, \theta, z, t) = -z\frac{\partial w_D(r, \theta, t)}{r\partial\theta}, \tag{1}$$
$$u_z(r, \theta, z, t) = w_D(r, \theta, t),$$

where u_r, u_θ and u_z are the displacements of a disk in r, θ and z directions, and u_D and w_D are the in-plane and the transverse displacements in the middle plane of a disk respectively. High rotational speed increases the in-plane displacement, radial stiffness and axial stiffness consecutively, and it increases the coupling effect between the transverse and in-plane displacements. This coupling effect leads to the non-linear dynamic characteristics of a disk at high speed. This non-linearity of the disk can be considered effectively by using von Karman non-linear strain–displacement relationship as follows:

$$\varepsilon_r = \frac{\partial u_r}{\partial r} + \frac{1}{2}\left(\frac{\partial u_z}{\partial r}\right)^2,$$
$$\varepsilon_\theta = \frac{u_r}{r} + \frac{\partial u_\theta}{r\partial\theta} + \frac{1}{2}\left(\frac{\partial u_z}{r\partial\theta}\right)^2,$$
$$\varepsilon_{r\theta} = \frac{\partial u_r}{r\partial\theta} + \frac{\partial u_\theta}{\partial r} - \frac{u_\theta}{r} + \frac{\partial u_z}{\partial r}\frac{\partial u_z}{r\partial\theta}, \tag{2}$$

where ε_r, ε_θ and $\varepsilon_{r\theta}$ are the strains in r and θ directions, and the shear strain respectively. Substituting equation (1) into equation (2) gives the following relationship:

$$\varepsilon_i = \bar{\varepsilon}_i - z\tilde{\varepsilon}_i (i = r, \theta, r\theta), \tag{3}$$

where $\bar{\varepsilon}$ and $z\tilde{\varepsilon}$ are the strain of the middle plane and the strain measured in the thickness direction from the middle plane of the disk respectively. Since the disk thickness is very thin, compared with the radial dimension, it can be assumed that the disk is in the state of plane stress as follows:

$$\begin{Bmatrix} \sigma_r \\ \sigma_\theta \\ \sigma_{r\theta} \end{Bmatrix} = \frac{E_D}{1 - v_D^2} \begin{bmatrix} 1 & v_D & 0 \\ v_D & 1 & 0 \\ 0 & 0 & \dfrac{1 - v_D}{2} \end{bmatrix} \begin{Bmatrix} \varepsilon_r \\ \varepsilon_\theta \\ \varepsilon_{r\theta} \end{Bmatrix}, \tag{4}$$

where E_D and v_D are Young's modulus and the Poisson ratio. Equation (4) can be rewritten as follows:

$$\sigma_i = \bar{\sigma}_i - z\tilde{\sigma}_i (i = r, \theta, r\theta). \tag{5}$$

From equations (3) and (5), the strain energy of a disk denoted by U_D can be expressed as follows:

$$U_D = \frac{1}{2} \int_V (\sigma_r \varepsilon_r + \sigma_\theta \varepsilon_\theta + \sigma_{r\theta} \varepsilon_{r\theta}) \, \mathrm{d}V \tag{6}$$

where V is the volume of a disk.

In Figure 2, the position vector of a point in the disk $\mathbf{R}_D$ is expressed as follows:

$$\mathbf{R}_D = \mathbf{r}_{D1} + \mathbf{r}_{D2}, \tag{7}$$

where $\mathbf{r}_{D1}$ and $\mathbf{r}_{D2}$ are the position vector from the inertial reference frame to the origin of local reference frame and the position vector of a point in the disk with respect to the local reference frame respectively. They can be expressed as follows:

$$\mathbf{r}_{D1} = X_D \mathbf{i}_1 + Y_D \mathbf{j}_1 + Z_D \mathbf{k}_1, \tag{8}$$

$$\mathbf{r}_{D2} = (r + u_r)(\cos\theta \, \mathbf{i}_2 + \sin\theta \, \mathbf{j}_2) + u_z \mathbf{k}_2, \tag{9}$$

where $\mathbf{i}_1$, $\mathbf{j}_1$ and $\mathbf{k}_1$ are the unit vectors of the inertial reference frame, and $\mathbf{i}_2$, $\mathbf{j}_2$ and $\mathbf{k}_2$ are the unit vectors of the local reference frame. X_D, Y_D and Z_D represent the translational displacements of the origin of the local reference frame with respect to the inertial reference frame, and r is the radial distance from the center of a disk to a point before elastic deformation. Velocity of a point in the disk $\mathbf{v}_D$ can be written as the time derivative of the position vector.

$$\mathbf{v}_D = \frac{\mathrm{d}\mathbf{R}_D}{\mathrm{d}t} = \dot{\mathbf{r}}_{D1} + {}^{O_2}\dot{\mathbf{r}}_{D2} + \omega_{O2} \times \mathbf{r}_{D2}, \tag{10}$$

where ${}^{O_2}\dot{\mathbf{r}}_{D2}$ is the time derivative with respect to the local reference frame and ω_{O2} is the angular velocity of the local reference frame expressed in terms of the local reference co-ordinates.

$$\omega_{O2} = \dot{\theta}_x \cos\theta_y \mathbf{i}_2 + \dot{\theta}_y \mathbf{j}_2 + \dot{\theta}_x \sin\theta_y \mathbf{k}_2, \tag{11}$$

where θ_x and θ_y are the Euler angles of the local reference frame. Using equations (1), (8), (9) and (11), equation (10) can be separated with respect to the disk thickness as follows:

$$\mathbf{v}_D = \bar{\mathbf{v}}_D - z\tilde{\mathbf{v}}_D. \tag{12}$$

Kinetic energy of disk, T_D can be approximated with the assumption of a thin disk as follows:

$$T_D = \frac{1}{2}\int \mathbf{v}_D \cdot \mathbf{v}_D \,\mathrm{d}m \approx \frac{1}{2}\rho_D h_D \int \bar{\mathbf{v}}_D \cdot \bar{\mathbf{v}}_D \mathrm{d}A \tag{13}$$

where ρ_D and h_D are the density and thickness of disk respectively.

Applying Hamilton's principle with equations (6) and (13) results in seven non-linear equations of the spinning disk under the coupled rigid body motion and elastic deformation. Under the assumption of the infinitesimal rigid body motion, derived equations can be linearized with respect to θ_x and θ_y as follows:

Equation for X_D is

$$\rho_D h_D \ddot{X}_D = 0. \tag{14}$$

Equation for Y_D is

$$\rho_D h_D \ddot{Y}_D = 0. \tag{15}$$

Equation for Z_D is

$$\rho_D h_D \left(\ddot{Z}_D + \frac{\partial^2 w_D}{\partial t^2} + 2\Omega \frac{\partial^2 w_D}{\partial \theta \partial t} + \Omega^2 \frac{\partial^2 w_D}{\partial \theta^2} \right) = 0. \tag{16}$$

Equation for θ_x is

$$\begin{aligned} &\rho_D h_D (\ddot{\theta}_x r^2 \sin^2\theta + \Omega \dot{\theta}_y r^2 + \Omega^2 w_D r \sin\theta) \\ &\quad + \rho_D h_D \left(\frac{\partial^2 w_D}{\partial t^2} + 2\Omega \frac{\partial^2 w_D}{\partial \theta \partial t} + \Omega^2 \frac{\partial^2 w_D}{\partial \theta^2} \right) r \sin\theta = 0. \end{aligned} \tag{17}$$

Equation for θ_y is

$$\begin{aligned} &\rho_D h_D (\ddot{\theta}_y r^2 \cos^2\theta - \Omega \dot{\theta}_x r^2 - \Omega^2 w_D r \cos\theta) \\ &\quad - \rho_D h_D \left(\frac{\partial^2 w_D}{\partial t^2} + 2\Omega \frac{\partial^2 w_D}{\partial \theta \partial t} + \Omega^2 \frac{\partial^2 w_D}{\partial \theta^2} \right) r \cos\theta = 0. \end{aligned} \tag{18}$$

Equation for u_D is

$$\frac{q_r - q_\theta}{r} + \frac{\partial q_r}{\partial r} + \rho_D h_D \Omega^2 r = 0. \tag{19}$$

Equation for w_D is

$$\begin{aligned} &\rho_D h_D \left(\ddot{Z}_D + \frac{\partial^2 w_D}{\partial t^2} + 2\Omega \frac{\partial^2 w_D}{\partial \theta \partial t} + \Omega^2 \frac{\partial^2 w_D}{\partial \theta^2} \right) \\ &\quad - \rho_D h_D \{ (\ddot{\theta}_x r \sin\theta - \ddot{\theta}_y r \cos\theta) + 2\Omega (\dot{\theta}_x r \cos\theta + \dot{\theta}_y r \sin\theta) \} \end{aligned}$$

$$+\frac{\partial}{r\partial r}\left\{r\left(q_r\frac{\partial w_D}{\partial r}\right)\right\}+\frac{\partial}{r\partial\theta}\left(q_\theta\frac{\partial w_D}{r\partial\theta}\right)-\frac{\partial}{r\partial r}\left\{r\left(\frac{M_r-M_\theta}{r}+\frac{\partial M_r}{\partial r}+2\frac{\partial M_{r\theta}}{r\partial\theta}\right)\right\}$$

$$-\frac{\partial}{r\partial\theta}\left(\frac{\partial M_\theta}{r\partial\theta}+2\frac{M_{r\theta}}{r}\right)=0, \tag{20}$$

where M_i and q_i $(i = r, \theta, r\theta)$ are the internal moments and the linearized internal forces in the middle plane of a disk and they are defined as follows:

$$M_i=\int_{-h/2}^{h/2} z\tilde{\sigma}_i\,\mathrm{d}z (i = r, \theta, r\theta), \tag{21}$$

$$\mathbf{q}=\mathbf{D}_1\bar{\varepsilon}^{linearized},$$

$$\mathbf{D_1}=\frac{E_D h_D}{1-v_D^2}\begin{bmatrix}1 & v_D & 0\\ v_D & 1 & 0\\ 0 & 0 & \dfrac{1-v_D}{2}\end{bmatrix}, \tag{22}$$

where $\bar{\varepsilon}^{linearized}$ is the linearized strain vector in the middle plane of a disk and it can be represented as follows:

$$[\bar{\varepsilon}_r\ \bar{\varepsilon}_\theta\ \bar{\varepsilon}_{r\theta}]^{\mathrm{T}}_{linearized}=\left[\frac{\partial u_D}{\partial r}\ \frac{u_D}{r}\ 0\right]^{\mathrm{T}}. \tag{23}$$

Equations (14) and (15) show that the rigid body translations of a disk in the in-plane directions are decoupled with the other co-ordinates. Equations (16)–(18) indicate that the axial rigid body translation and the rigid body tilting motion are coupled with the transverse displacement of a disk. Equation (19) is derived with the assumption that transverse displacement has little influence on in-plane displacement so that it can be a linear equation in terms of the in-plane displacement u_D. Equation (20) shows that in-plane and transverse displacements of a disk are coupled with the axial rigid body translation and the rigid body tilting motion and it is a non-linear equation. This non-linear equation makes the whole set of equations complicated. However, u_D can be directly determined by solving equation (19) and the linearized internal forces q_r, q_θ can be calculated. Then, equation (20) becomes a linear equation with respect to the transverse displacement w_D at constant angular speed.

2.2. EQUATIONS OF MOTION FOR A ROTATING SPINDLE AND A STATIONARY SHAFT

Rayleigh beam considering the rotary inertia effect can model a rotating spindle, and its governing equations considering the axial rigid translation are expressed as follows [6]:

Equation for u_H is

$$\rho_H\left(A_H\frac{\partial^2 u_H}{\partial t^2}-I_H\frac{\partial^4 u_H}{\partial t^2\partial z^2}-2I_H\Omega\frac{\partial^3 v_H}{\partial t\,\partial z^2}\right)+\frac{\partial^2 M_x}{\partial z^2}=0. \tag{24}$$

Equation for v_H is

$$\rho_H\left(A_H\frac{\partial^2 v_H}{\partial t^2}-I_H\frac{\partial^4 v_H}{\partial t^2\,\partial z^2}+2I_H\Omega\frac{\partial^3 u_H}{\partial t\,\partial z^2}\right)+\frac{\partial^2 M_y}{\partial z^2}=0. \tag{25}$$

Equation for Z_H is

$$m_H\ddot{Z}_H=0, \tag{26}$$

where u_H, v_H and Z_H are the bending deformations in x_1 and y_1 directions, and the rigid body translation in z_1 direction respectively. ρ_H, $\mathrm{A_H}$ and I_H are the density, cross-sectional area, and second areal moment of inertia of a spindle respectively. M_x and M_y are the internal moments of the spindle defined as follows:

$$M_x=E_HI_H\frac{\partial^2 u_H}{\partial x^2},\qquad M_y=E_HI_H\frac{\partial^2 v_H}{\partial y^2} \tag{27}$$

where E_H is Young's modulus of spindle.

The stationary shaft supporting the disk–spindle–bearing system is modelled by a Euler beam. Its equations of motion are similar to those of the rotating spindle except that the rotary inertia effect is excluded.

Equation for u_S is

$$\rho_SA_S\frac{\partial^2 u_S}{\partial t^2}+\frac{\partial^2 M_x}{\partial z^2}=0. \tag{28}$$

Equation for v_S is

$$\rho_SA_S\frac{\partial^2 v_S}{\partial t^2}+\frac{\partial^2 M_y}{\partial z^2}=0, \tag{29}$$

where u_S and v_S are the bending deformation of shaft in x_1, y_1 and y_1 directions respectively. ρ_S and A_S are the density and cross-sectional area of the shaft respectively.

3. DISCRETIZATION BY FINITE ELEMENTS

Galerkin's method is used to solve the partial differential equations of motion of the disk, spindle and shaft determined in the previous section. The weak form of equations (14)–(20) of the disk is expressed as follows:

$$\begin{Bmatrix}W_1\\W_2\\W_3\\W_4\\W_5\end{Bmatrix}^{\mathrm{T}}\begin{bmatrix}m_D&0&0&0&0\\0&m_D&0&0&0\\0&0&m_D&0&0\\0&0&0&I_D&0\\0&0&0&0&I_D\end{bmatrix}\begin{Bmatrix}\ddot{\psi}_1\\\ddot{\psi}_2\\\ddot{\psi}_3\\\ddot{\psi}_4\\\ddot{\psi}_5\end{Bmatrix}$$

$$+\Omega\begin{Bmatrix}W_4\\W_5\end{Bmatrix}^{\mathrm{T}}\begin{bmatrix}0&2I_D\\-2I_D&0\end{bmatrix}\begin{Bmatrix}\dot{\psi}_4\\\dot{\psi}_5\end{Bmatrix}$$

$$
\begin{aligned}
&+\int_{\Omega}\begin{Bmatrix}W_3\\W_6\end{Bmatrix}^{\mathrm{T}}\begin{bmatrix}0 & \rho_D h_D\\ \rho_D h_D & 0\end{bmatrix}\begin{Bmatrix}\ddot{\psi}_3\\ \ddot{\psi}_6\end{Bmatrix}\mathrm{d}\Omega\\
&+\rho_D h_D\int_{\Omega}\begin{Bmatrix}W_4\\W_5\\W_6\end{Bmatrix}^{\mathrm{T}}\begin{bmatrix}0 & 0 & r\sin\theta\\ 0 & 0 & -r\cos\theta\\ r\sin\theta & -r\cos\theta & 0\end{bmatrix}\begin{Bmatrix}\ddot{\psi}_4\\ \ddot{\psi}_5\\ \ddot{\psi}_6\end{Bmatrix}\mathrm{d}\Omega\\
&+2\rho_D h_D\Omega\int_{\Omega}\begin{Bmatrix}W_4\\W_5\\W_6\end{Bmatrix}^{\mathrm{T}}\begin{bmatrix}0 & 0 & -r\cos\theta\\ 0 & 0 & -r\sin\theta\\ r\cos\theta & r\sin\theta & 0\end{bmatrix}\begin{Bmatrix}\dot{\psi}_4\\ \dot{\psi}_5\\ \dot{\psi}_6\end{Bmatrix}\mathrm{d}\Omega\\
&+\rho_D h_D\int_{\Omega}W_6\ddot{\psi}_6\mathrm{d}\Omega\\
&+\rho_D h_D\Omega\int_{\Omega}\left(W_6\frac{\partial\dot{\psi}_6}{\partial\theta}-\frac{\partial W_6}{\partial\theta}\dot{\psi}_6\right)\mathrm{d}\Omega\\
&+\int_{\Omega}\begin{Bmatrix}-\rho_D h_D\Omega^2\dfrac{\partial W_6}{\partial\theta}\dfrac{\partial\psi_6}{\partial\theta}\\ +\tilde{\varepsilon}(W_6)^{\mathrm{T}}\mathbf{D}_2\tilde{\varepsilon}(\psi_6)\\ +\rho_D h_D\Omega^2\dfrac{\partial W_6}{\partial r}r\psi_6\\ -\tilde{\varepsilon}(W_6)^{\mathrm{T}}\mathbf{D}_2\bar{\varepsilon}^{linearized}(\psi_7)\psi_6\end{Bmatrix}\mathrm{d}\Omega\\
&-\int_{\Omega}\{\bar{\varepsilon}^{linearized}(W_7)^{\mathrm{T}}\mathbf{D}_1\bar{\varepsilon}^{linearized}(\psi_7)\}\mathrm{d}\Omega\\
&=-\rho_D h_D\Omega^2\int_{\Omega}W_7 r\,\mathrm{d}\Omega,
\end{aligned}
\tag{30}
$$

where $\psi_i (i = 1, 2, \ldots, 7)$ are the approximate solutions corresponding to X_D, Y_D, Z_D, θ_x, θ_y, w_D and u_D, respectively, and $W_i (i = 1, 2, \ldots, 7)$ are the weighting functions to minimize the residuals.

As shown in Figure 3, the annular sector element is used to discretize the disk. Since it has the curved boundaries, it is appropriate to analyze the circular disk and it gives satisfactory solutions with a small number of elements [7]. The shape function of the transverse displacement uses a conforming Hermite interpolation function ($\mathbf{N}_6$) which satisfies the continuity of slope and the twist condition at a node. Lagrange interpolation function ($\mathbf{N}_7$) is also used as a shape function of in-plane displacement. Displacement in an annular sector element can be interpolated using the shape functions and displacements of nodes as follows:

$$
\begin{aligned}
\psi_i &= N_i d_i (i = 1, 2, \ldots, 5),\\
\psi_6 &= \mathbf{N}_6\mathbf{d}_6,\\
\psi_7 &= \mathbf{N}_7\mathbf{d}_7.
\end{aligned}
\tag{31}
$$

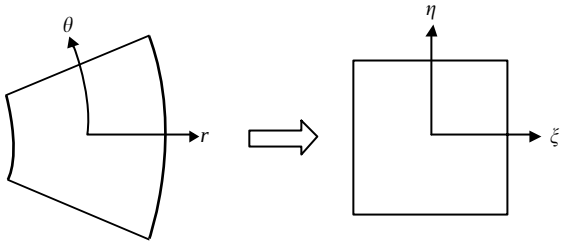

Figure 3. Annular sector element.

Since $\psi_i (i = 1, 2, \ldots, 5)$ corresponds to the rigid body displacement, $N_i (1, 2, \ldots, 5)$ becomes 1. Nodal displacements $\mathbf{d}_6$ and $\mathbf{d}_7$, corresponding to the transverse and in-plane displacements, are expressed as follows:

$$\mathbf{d}_6 = \left[w_1 \quad \frac{\partial w_1}{\partial r} \quad \frac{\partial w_1}{\partial \theta} \quad \frac{\partial w_1}{\partial r \partial \theta} \quad \cdots \quad \frac{\partial w_4}{\partial r \partial \theta} \right]_e^{\mathrm{T}},$$
$$\mathbf{d}_7 = [u_1 \quad u_2 \quad u_3 \quad u_4]_e^{\mathrm{T}}. \tag{32}$$

The following element matrix equations of the disk can be obtained after substituting equation (31) into equation (30):

$$\mathbf{m}_D^1 = \begin{bmatrix} m_D & 0 & 0 & 0 & 0 \\ 0 & m_D & 0 & 0 & 0 \\ 0 & 0 & m_D & 0 & 0 \\ 0 & 0 & 0 & I_D & 0 \\ 0 & 0 & 0 & 0 & I_D \end{bmatrix}, \tag{33}$$

$$\mathbf{g}_D^1 = \Omega \begin{bmatrix} 0 & 2I_D \\ -2I_D & 0 \end{bmatrix}, \tag{34}$$

$$\mathbf{m}_D^2 = \rho_D h_D \int_{\Omega^e} \mathbf{N}_6^{\mathrm{T}} \mathrm{d}\Omega, \tag{35}$$

$$\mathbf{m}_D^3 = \rho_D h_D \int_{\Omega^e} \begin{Bmatrix} -r \sin\theta \\ r \cos\theta \end{Bmatrix} \mathbf{N}_6^{\mathrm{T}} \mathrm{d}\Omega, \tag{36}$$

$$\mathbf{g}_D^2 = 2\rho_D h_D \Omega \int_{\Omega^e} \begin{Bmatrix} r \cos\theta \\ r \sin\theta \end{Bmatrix} \mathbf{N}_6^{\mathrm{T}} \mathrm{d}\Omega, \tag{37}$$

$$\mathbf{m}_D^4 = \rho_D h_D \int_{\Omega^e} \mathbf{N}_6 \mathbf{N}_6^{\mathrm{T}} \mathrm{d}\Omega, \tag{38}$$

$$\mathbf{g}_D^3 = \rho_D h_D \Omega \int_{\Omega^e} \left(\mathbf{N}_6 \frac{\partial \mathbf{N}_6^{\mathrm{T}}}{\partial \theta} - \frac{\partial \mathbf{N}_6}{\partial \theta} \mathbf{N}_6^{\mathrm{T}} \right) \mathrm{d}\Omega, \tag{39}$$

$$\mathbf{k}_D^1 = \int_{\Omega^e} \tilde{\varepsilon}^{\mathrm{T}} \mathbf{D}_2 \tilde{\varepsilon} \, \mathrm{d}\Omega, \tag{40}$$

$$\mathbf{k}_D^2 = -\rho_D h_D \Omega^2 \int_{\Omega^e} \frac{\partial \mathbf{N}_6}{\partial \theta} \frac{\partial \mathbf{N}_6^{\mathrm{T}}}{\partial \theta} \, \mathrm{d}\Omega, \tag{41}$$

$$\mathbf{k}_D^3 = \rho_D h_D \Omega^2 \int_{\Omega^e} \frac{\partial \mathbf{N}_6}{\partial r} r \mathbf{N}_6^{\mathrm{T}} \mathrm{d}\Omega, \tag{42}$$

$$\mathbf{k}_D^4 = -\int_{\Omega^e} \tilde{\varepsilon}^{\mathrm{T}} \mathbf{D}_2 \bar{\varepsilon}^{linearized} \mathbf{N}_6^{\mathrm{T}} \mathrm{d}\Omega, \tag{43}$$

$$\mathbf{k}_D^5 = -\int_{\Omega^e} \bar{\varepsilon}^{linearized\,\mathrm{T}} \mathbf{D}_1 \bar{\varepsilon}^{linearized} \, \mathrm{d}\Omega, \tag{44}$$

$$\mathbf{f}_D = -\rho_D h_D \Omega^2 \int_{\Omega^e} \mathbf{N}_7 r \, \mathrm{d}\Omega, \tag{45}$$

$$\mathbf{D}_2 = \frac{E_D h_D^3}{12(1 - v_D^2)} \begin{bmatrix} 1 & v_D & 0 \\ v_D & 1 & 0 \\ 0 & 0 & \dfrac{1 - v_D}{2} \end{bmatrix}, \tag{46}$$

where m_D and I_D are the mass and mass moment of inertia of the disk respectively. Equation (33) is the inertia matrix corresponding to the rigid body motions (X_D, Y_D, Z_D, θ_x, θ_y), and equation (34) is the element gyroscopic matrix corresponding to the rigid body tilting (θ_x, θ_y). Equation (35) is the element mass matrix coupled with the axial rigid translation and transverse displacement. Equations (36) and (37) are the element mass matrix and element gyroscopic matrix coupled with the rigid body tilting and transverse displacement. Equations (38)–(40) are the element mass matrix, element gyroscopic matrix, and element stiffness matrix due to the transverse displacement respectively. Equations (41) and (42) are the element stiffness matrices due to the disk rotation. Equation (43) is the element stiffness matrix coupled with the transverse and in-plane displacements. Equation (44) is the element iffness matrix due to the in-plane displacement of a disk and equation (45) is the element force vector due to the centrifugal force by the disk rotation.

The element matrix of the rotating spindle can also be obtained by using Galerkin's method as follows:

$$\mathbf{m}_H^t = \int_z \mathbf{N}_8 \mathbf{C}_1 \mathbf{N}_8^{\mathrm{T}} \mathrm{d}z, \tag{47}$$

$$\mathbf{m}_H^r = \int_z \frac{\partial \mathbf{N}_8}{\partial z} \mathbf{C}_2 \frac{\partial \mathbf{N}_8^{\mathrm{T}}}{\partial z} \, \mathrm{d}z, \tag{48}$$

$$\mathbf{g}_H = \Omega \int_z \frac{\partial \mathbf{N}_8}{\partial z} \mathbf{C}_3 \frac{\partial \mathbf{N}_8^{\mathrm{T}}}{\partial z} \mathrm{d}z, \tag{49}$$

$$\mathbf{k}_H = \int_z \frac{\partial^2 \mathbf{N}_8}{\partial z^2} \mathbf{C}_4 \frac{\partial^2 \mathbf{N}_8^{\mathrm{T}}}{\partial z^2} \mathrm{d}z, \tag{50}$$

$$\mathbf{C}_1 = \begin{bmatrix} \rho_H A_H & 0 \\ 0 & \rho_H A_H \end{bmatrix},$$

$$\mathbf{C}_2 = \begin{bmatrix} \rho_H I_{\mathrm{H}} & 0 \\ 0 & \rho_H I_H \end{bmatrix},$$

$$\mathbf{C}_3 = \begin{bmatrix} 0 & 2\rho_H I_H \\ -2\rho_H I_H & 0 \end{bmatrix}, \tag{51}$$

$$\mathbf{C}_4 = \begin{bmatrix} E_H I_H & 0 \\ 0 & E_H I_H \end{bmatrix},$$

where $\mathbf{N}_8$ is the shape function of a beam element. Equations (47) and (48) are the element mass matrices due to the bending deformation and rotary inertia effect respectively. Equations (49) and (50) are the element gyroscopic matrix and element stiffness matrix of the spindle respectively.

The element matrix of the stationary shaft can be obtained by neglecting the element mass and gyroscopic matrix due to the rotary inertia effect in the element matrix of the rotating spindle as follows:

$$\mathbf{m}_S = \int_z \mathbf{N}_8 \mathbf{C}_5 \mathbf{N}_8^{\mathrm{T}} \mathrm{d}z, \tag{52}$$

$$\mathbf{k}_S = \int_z \frac{\partial^2 \mathbf{N}_8}{\partial z^2} \mathbf{C}_6 \frac{\partial^2 \mathbf{N}_8^{\mathrm{T}}}{\partial z^2} \mathrm{d}z. \tag{53}$$

Equations (52) and (53) are the element mass matrix and element stiffness matrix of a stationary shaft. Matrices $\mathbf{C}_5$ and $\mathbf{C}_6$ have the same elements as those of $\mathbf{C}_1$ and $\mathbf{C}_4$ in equation (51).

4. SUBSTRUCTURE SYNTHESIS

Finite element equations of each substructure of the disk–spindle–bearing–shaft system derived from each local reference frame must satisfy the geometric compatibility in the internal boundaries where each substructure is connected before an entire system is assembled [8, 9]. As shown in the following equations (54) and (55), the rigid body translation and tilting motion of the disk must equal to the bending deformation in x and y direction, axial rigid body motion and rotary motion of the spindle where the disk is

connected to the spindle.

$$X_D = u_H^d, \quad Y_D = v_H^d, \quad Z_D = Z_H^d, \tag{54}$$

$$\theta_x = -\frac{\partial v_H^d}{\partial z}, \quad \theta_y = \frac{\partial u_H^d}{\partial z}, \tag{55}$$

where superscript d denotes the deformation of the spindle at which the disk is connected.

Using the element matrix equations derived in the previous chapter and the geometric constraint equations in (54) and (55), the matrix–vector equation of the entire system can be expressed as follows:

$$\mathbf{M}\ddot{\mathbf{x}} + \mathbf{G}\dot{\mathbf{x}} + \mathbf{K}\mathbf{x} = \mathbf{0}, \tag{56}$$

$$\mathbf{M} = \begin{bmatrix} \mathbf{M}_H + \mathbf{M}_D^1 & \mathbf{M}_D^3 & \mathbf{0} & \mathbf{0} \\ & \mathbf{M}_D^4 & \mathbf{M}_D^2 & \mathbf{0} \\ \textit{symm.} & & m_H + m_D & 0 \\ & & & \mathbf{M}_S \end{bmatrix}, \tag{57}$$

$$\mathbf{G} = \begin{bmatrix} \mathbf{G}_H + \mathbf{G}_D^1 & \mathbf{G}_D^2 & \mathbf{0} & \mathbf{0} \\ & \mathbf{G}_D^3 & \mathbf{0} & \mathbf{0} \\ \textit{skew}-\textit{ymm.} & & 0 & 0 \\ & & 0 & \mathbf{0} \end{bmatrix}, \tag{58}$$

$$\mathbf{K} = \begin{bmatrix} \mathbf{K}_H & \mathbf{0} & \mathbf{0} & \mathbf{0} \\ & \mathbf{K}_D & \mathbf{0} & \mathbf{0} \\ \textit{symm.} & & 0 & 0 \\ & & & \mathbf{K}_S \end{bmatrix} + \mathbf{K}_{BR}, \tag{59}$$

where **M**, **G** and **K** are the global mass, gyroscopic and stiffness matrix of the entire system respectively. The stiffness of ball bearings is determined by A. B. Jones' theory considering the five degrees of freedom of a general rotor–bearing system [10]. The subscripts H, D, S and BR correspond to the assembled matrices of the spindle, disk, shaft and bearing respectively. The superscript 1, 2, 3 and 4 represent the intermediate element mass and gyroscopic matrices defined in equations (33)–(44).

5. RESULTS AND DISCUSSION

5.1. FINITE ELEMENT MODEL

Equation (56) is transformed to the state space matrix–vector equation, and the associated eigenvalue problem is solved by QR iterative method. A computer program is developed to analyze the natural frequencies of a disk–spindle–bearing–shaft system in an HDD as shown in Figure 1. This model is composed of three disks, a spindle, two ball bearings and a shaft. Figure 4 shows the finite element model of each disk and a spindle–bearing–shaft system. Each disk is divided into 32 annular sector elements (2×16 in radial and circumferential directions, respectively) and it has 240 degrees of freedom. The spindle and shaft are divided into 16 Rayleigh beam elements and eight Euler beam elements, and they have 68 and 36 degrees of freedom respectively. Clamp, spacers, yoke

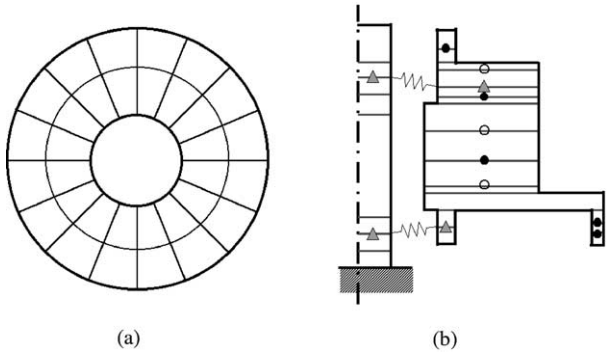

Figure 4. Finite element model of a disk (a) and a spindle–bearing–shaft system (b).

TABLE 2

Major design variables of a disk–spindle–bearing–shaft system in an HDD

Mode	Disk	Spindle	Stationary shaft	Magnet	Spacer
Inner radius	1·5e − 2				1·25e − 2
Outer radius	4·75e − 2				1·65e − 2
Height	8·0e − 4	1·30e − 3	1·65e − 2	3·5e − 3	2·75e − 3
Density	2·75e3	2·75e3	7·8e3	5·998e3	2·75e3
Young's modulus	7·2e10	7·2e10	2·0e11	1·7e11	7·2e10
Poisson ratio	0·34	0·33	0·3	0·3	0·33

and permanent magnet are assumed as rigid bodies so that their mass and moment of inertia are added to the element mass matrix of the spindle. Black dots represent the nodes corresponding to the clamp, two spacers, yoke and magnet. Three circles represent the nodes in the spindle where the disk is connected. Triangles represent the nodes at which the spindle and the shaft are connected by ball bearings. The entire system has a total of 824 degrees of freedom. Table 2 shows the major design parameters.

5.2. EXPERIMENTAL VERIFICATION

Figure 5 shows the comparison of the simulation and experimental results of the natural frequencies in the HDD spindle system due to the variation of the rotational speed up to 10 000 r.p.m. Modal testing is performed to verify the simulation result. The experimental results are obtained through the impact hammer test of a 3·5 in HDD spindle system, which is fixed on the vibration isolation table after the cover is removed. Laser doppler vibrometer is used to measure the velocity of the out-of-plane motion of a disk. Then, frequency response functions are obtained for the stationary HDD spindle system as well as the rotating HDD spindle system by changing the rotation speed from 42 to 168 Hz by the increment of 6 Hz. Simulation results agree very well with the experimental ones as shown in Figure 5. $B(M, \mathrm{N})$ and $U(M, N)$ represent the balanced and unbalanced modes with M nodal circles and N nodal diameters [2]. Subscript b and f denote the backward and forward precession modes respectively. $U(0, 0)$ is the unbalanced mode coupled with the axial rigid body translation of the spindle and disk mode, and $B(0, 0)$ is the conventional

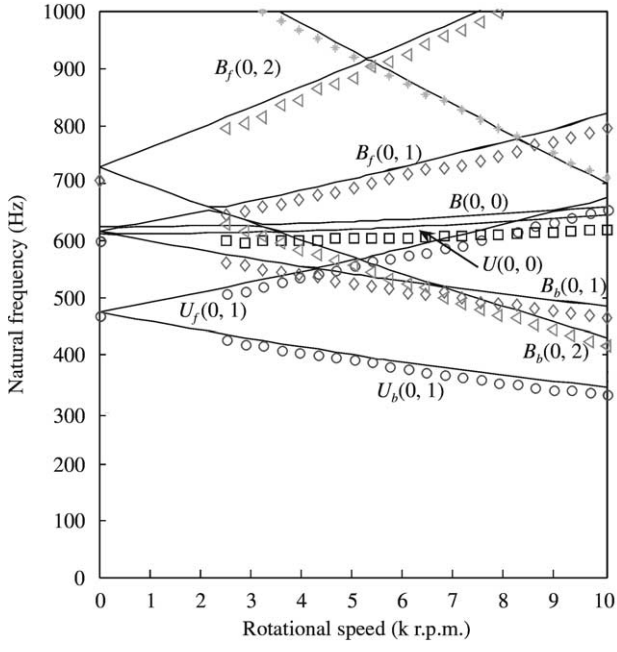

Figure 5. Comparison of natural frequencies between numerical and experimental results: ——, numerical result; □, experimental result.

balanced disk mode. Figure 6 shows the four vibration mode shapes of the HDD spindle system. In the modal testing, the natural frequency of unbalanced $U(0,0)$ mode cannot be separated from the balanced $B(0,0)$ mode. Those modes are very close to each other as indicated by Shen and Ku [2]. In simulation, the frequency difference between two modes is around 13 Hz. Figure 7 shows the frequency response function at the rotating speed of 5400 r.p.m., and Table 3 shows the comparison of the simulation and experimental results at this speed. The results agree within 5% error.

5.3. COUPLED VIBRATION MODE IN A DISK–SPINDLE–BEARING–SHAFT SYSTEM

Figure 8 shows the natural frequencies of a spinning disk only with fixed boundary condition at the inner radius of a disk (a) and a spinning disk–spindle system supported by bearing and shaft (b) due to the variation of rotational speed. All natural frequencies of a spinning disk case exactly match with those of a disk–spindle–bearing–shaft system except those two frequencies. Spindle–bearing–shaft produces two additional vibration frequencies, i.e., $U(0, 1)$ mode in forward and backward directions and $U(0,0)$ mode which are only observed in a disk–spindle–bearing–shaft system. They are coupled modes between the disk and spindle–bearing–shaft system. They can be clearly explained by the vibration mode shape as well as the governing equations of a disk with rigid body motion. As shown in Figure 6(a), $U(0,1)$ mode is a rocking vibration mode coupled with the transverse displacement of a disk and rigid body tilting motion of a spindle, and it can be predicted and explained by the coupled governing equation of a disk in equations (17) and (18). As shown in Figure 6(c), $U(0,0)$ mode is an axial vibration mode coupled with the transverse displacement of a disk and axial rigid body motion of the spindle, and it can be also predicted and explained by the coupled governing equation of a disk in equation (16).

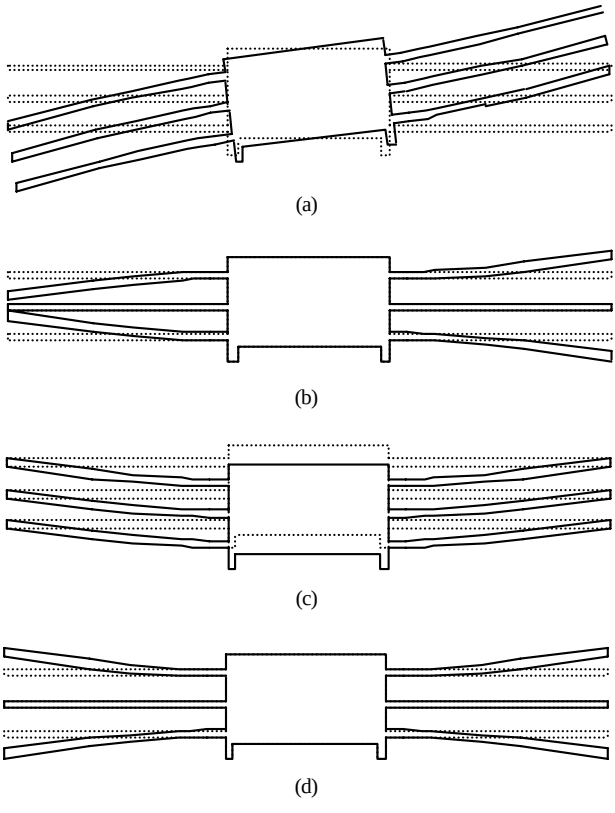

Figure 6. Mode shapes of disk–spindle system. (a) $U(0,1)$ mode; (b) $B(0,1)$ mode; (c) $U(0,0)$ mode; (d) $B(0,0)$ mode.

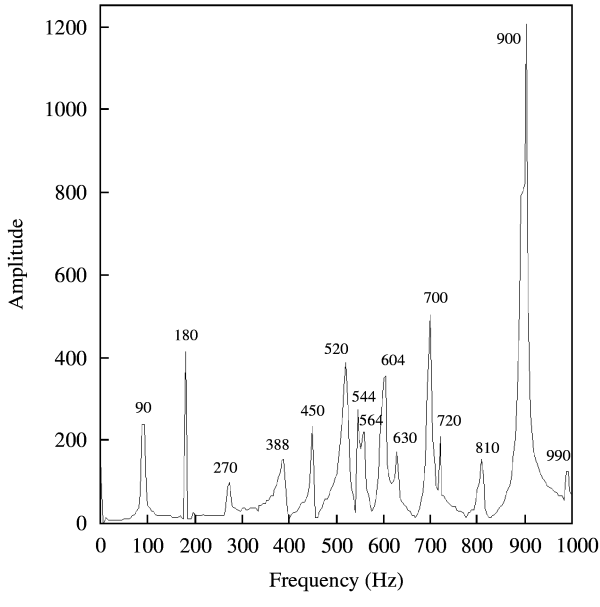

Figure 7. Frequency response function at 5400 r.p.m.

TABLE 3

Comparison of natural frequencies between numerical and experimental results ($\Omega = 5400$ r.p.m.)

Mode		Analysis (Hz)	Experiment (Hz)	Error (%)
1	U_b (0, 1)	396	388	2·02
2	B_b (0, 1)	536	520	2·99
3	U_f (0, 1)	574	564	1·74
4	B_b (0, 2)	560	544	2·86
5	U (0, 0)	622	604	2·89
6	B (0, 0)	635	604	4·88
7	B_f (0, 1)	716	700	2·23

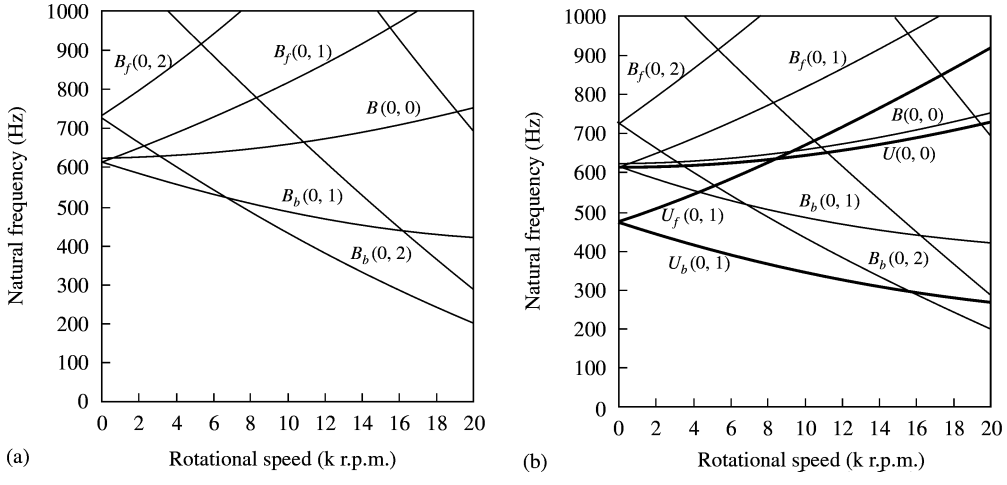

Figure 8. Natural frequencies of a disk (a) and a disk–spindle–bearing–shaft system (b).

5.4. EFFECT OF DISK NON-LINEARITY

Figure 9 shows the variation of natural frequencies due to the effect of disk non-linearity. Discrepancy between linear and non-linear models increases with the increase of the rotational speed. Natural frequencies increase linearly up to 6000 r.p.m., and then they change non-linearly. High rotational speed increases the coupling effect between the transverse and in-plane displacements, and it increases the in-plane displacement, radial stiffness and axial stiffness consecutively. In 2000, the fastest rotational speed of a high-capacity HDD is 15 000 r.p.m. so that disk non-linearity should be considered to predict the natural frequencies of an HDD spindle system accurately.

5.5 EFFECT OF THE ROTATING SPINDLE AND STATIONARY SHAFT FLEXIBILITY

Flexibility of the stationary shaft has not been included in the prior researches to analyze the natural frequencies of HDD spindle system [2–5]. Figure 10(a)–(d) shows the natural

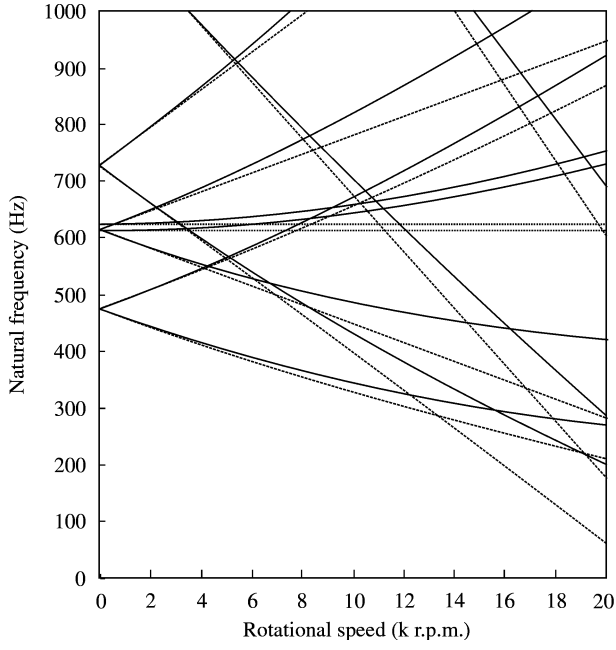

Figure 9. Natural frequencies due to disk non-linearity: ——, nonlinear model; ·····, linear model.

frequencies of the disk–spindle–bearing–shaft system when both spindle and shaft are flexible; when spindle is flexible but shaft is rigid; when spindle is rigid but shaft is flexible; when both spindle and shaft are rigid. Rigid spindle or shaft assumes to have 100 times stiffer Young's modulus than flexible spindle or shaft. Natural frequencies except $U(0, 1)$ mode do not change due to the flexibility of the rotating spindle and stationary shaft. Compared with Figure 10(a) and (b) or (c) and (d), shaft flexibility lowers the frequency of $U(0, 1)$ mode, i.e., 50 Hz in this case. Shen and Ku indicated the several possible causes of the discrepancy of $U(0, 1)$ mode between their simulation and experimental results [2]. This research shows that shaft flexibility may be the critical parameter to predict the natural frequencies of the unbalanced $U(0, 1)$ mode accurately. Compared with Figure 10(a) and (c) or (b) and (d), spindle flexibility has no influence on the vibration characteristics of this HDD disk–spindle–bearing–shaft system.

5.6. EFFECT OF SHAFT BOUNDARY CONDITION

The results in Figures 5, 7–10 are obtained from the analysis of an HDD spindle system with free–fixed boundary condition of the stationary shaft, which is popular design of a 2·5 in or smaller size of HDD spindle system. In most 3.5 in HDD spindle systems, the stationary shaft is fixed to a top cover with a bolt so that it can be assumed as a beam with fixed–fixed boundary condition. Figure 11 shows natural frequencies of a disk–spindle–bearing–shaft system with fixed–fixed boundary condition of a stationary shaft. Compared with Figure 10(a), every natural frequency except $U(0, 1)$ mode does not change in both free–fixed and fixed-fixed boundary condition. Fixed-fixed boundary condition of a short shaft makes the flexible shaft stiff or rigid so that it increases the natural frequency of $U(0, 1)$ mode. In this model, fixed–fixed boundary condition of a shaft produces the same result as shown in Figure 10(b) and (d) as if it is a rigid shaft.

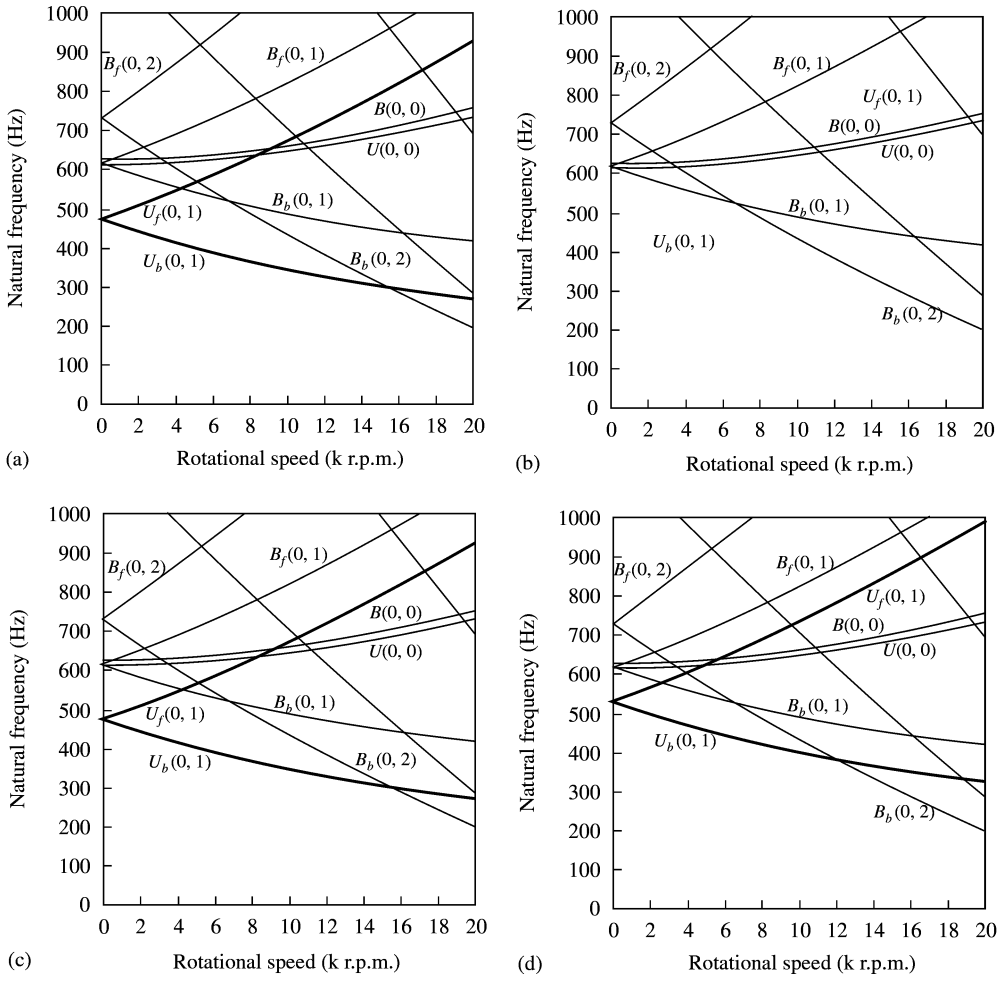

Figure 10. Natural frequencies due to the effect of the spindle and shaft flexibility. (a) flexible spindle and shaft; (b) flexible spindle and rigid shaft; (c) rigid spindle and flexible shaft; (d) rigid spindle and shaft.

6. CONCLUSIONS

The proposed method in this paper can be effectively applied to predict the natural frequencies of a disk–spindle–bearing–shaft system in the various forms of computer storage devices, i.e., FDD, CD, HDD and DVD. The major results are as follows:

1. The equations of motion for a spinning, flexible disk that undergoes the coupled infinitesimal rigid body motion and elastic deformation are derived by Hamilton's principle.
2. FEM and substructure synthesis are used to analyze the natural frequencies of a spinning flexible disk–spindle system supported by bearing and flexible shaft. The finite element equations of each substructure are derived, and the entire system including every component is assembled consistently by satisfying the geometric compatibility at the internal boundaries.

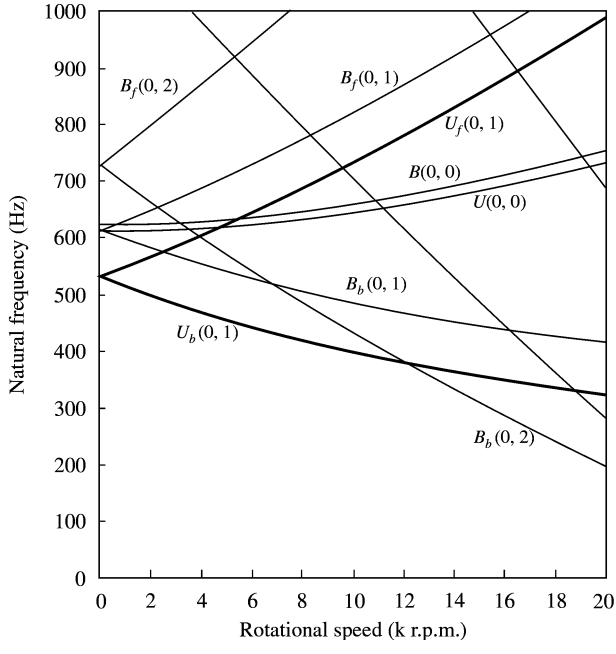

Figure 11. Natural frequencies with the fixed top boundary condition of a stationary shaft.

3. In an HDD spindle system, the flexibility and boundary conditions of a shaft are the critical parameters to predict the natural frequencies of $U(0, 1)$ mode accurately. But the spindle flexibility has no influence on $U(0,1)$ mode.

REFERENCES

1. J. A. DOPKIN and T. E. SHOUP 1974 *Journal of Engineering for Industry* **96**, 1328–1333. Rotor resonant speed reduction caused by flexibility of disks.
2. I. Y. SHEN and C.-P. R. KU 1997 *Journal of Applied Mechanics* **64**, 165–174. A nonclassical vibration analysis of a multiple rotating disk and spindle assembly.
3. C.-W LEE and S.-B. CHUN 1998 *Journal of Vibration and Acoustics* **120**, 87–94. Vibration analysis of a rotor with multiple flexible disks using assumed modes method.
4. C.-W. LEE, H. S. JIA, C.-S. KIM and S.-B. CHUN 1997 *Journal of Sound and Vibration* **207**, 435–451. Tuning of simulated natural frequencies for a flexible shaft-multiple flexible disk system.
5. S. LIM 2000 *Journal of Sound and Vibration* **233**, 601–616. Finite element analysis of flexural vibrations in hard disk drive spindle systems.
6. H. D. NELSON and J. M. MCVAUGH 1976 *Journal of Engineering for Industry* **98**, 593–600. The dynamics of rotor-bearing systems using finite elements.
7. M. D. OLSON and G. M. LINDBERG 1970 *International Journal of Mechanical Sciences* **12**, 17–33. Annular and circular sector finite elements for plate bending.
8. A. L. HALE and L. MEIROVITCH 1980 *Journal of Sound and Vibration* **69**, 309–326. A general substructure synthesis method for the dynamic simulation of complex structures.
9. L. MEIROVITCH 1980 *Computational Methods in Structural Dynamics*. Alphen aan den Rijn, The Netherlands: Sijthoff-Noordhoff International Publishers.
10. G. H. JANG, D. K. JUNG, N. Y. PARK and J. S. PARK 1996 *Proceedings of Incremental Motion Control Systems and Devices*, 167–174. Analysis of the dynamic characteristics of ball bearing in 3·5 inch HDD spindle motor.